Remote Sensing of Environment 114 (2010) 1590–1601

Contents lists available at ScienceDirect

Remote Sensing of Environment

journal homepage: www.elsevier.com/locate/rse

Oil spill detection from SAR intensity imagery using a marked point process

Yu Li, Jonathan Li *

University of Waterloo, Department of Geography and Environmental Management, 200 University Avenue West, Waterloo, Ontario, Canada N2L 3G1

ARTICLE INFO

Article history:
Received 17 July 2009
Received in revised form 11 January 2010
Accepted 20 February 2010

Keywords:
Oil spill
Dark spot detection
Marked point process
Bayesian inference
Reversible Jump Markov Chain Monte Carlo (RJMCMC)
Maximum a posteriori (MAP)

ABSTRACT

This paper presents a new algorithm for the detection of oil spill from SAR intensity images. The proposed algorithm combines the marked point process, Bayesian inference and Markov Chain Monte Carlo (MCMC) technique. In this paper, the candidates of oil spills or dark spots in a SAR intensity image are characterized by a Poisson marked point process. The marked point process is formed by a group of random points (as a point process modelling the locations of oil spills) and a set of parameters including geometric parameters of windows centred at the random points and gamma distribution parameters (as the marks attaching to each point). As a result, the candidates of oil spills are represented by a group of windows, in which the intensities of pixels follow independent and identical gamma distribution with lower mean than that for the identical gamma distribution of the pixels out of windows. Following the Bayesian paradigm, the posterior distribution, which characterizes the locations and statistical distributions of oil spills, can be obtained up to a normalizing constant. In order to simulate from the posterior distribution and to estimate the parameters of the posterior distribution, the Revisable Jump MCMC (RJMCMC) algorithm is used. The optimal locations and sizes of dark spots are obtained by a maximum a posteriori (MAP) algorithm. The proposed approach is tested using Radarsat-1 SAR images with oil spills indicated by human analysts. The results show that the proposed approach works well and is very promising.

1. Introduction

The ocean plays an important role in regulating the Earth's environment and the global climate, as well as providing resources for mankind. Human activities are increasingly changing the ocean and its delicate balance. Oil pollution belongs to the most widespread man-caused emergency situations considerably harming ocean ecosystems and different types of economic activities. Earth observation satellite sensors have proved to be a cost-effective, all-weather and all-day early warning way to help identify and monitor oil-spills before they cause widespread damage. Currently, there are many space-borne remote sensing sensors that have been used for oil spill monitoring, examples including microwave sensors such as synthetic aperture radar (SAR), Infrared (IR) sensors (Fingas & Brown, 1997), and ultraviolet (UV) sensors (Fingas & Brown, 1997). Among of them, SAR sensors with all weather, day and night, large area observation capabilities are a convenient and effective tool for oil spill monitoring. The commonly used SAR sensors for this purpose include RADARSAT-1, ENVISAT, ERS-1 and ERS-2 (Brekke & Solberg, 2005; Topouzelis, 2008).

The detectability of oil spill by SAR sensors is based on the fact that oil slicks dampen the Bragg waves on the ocean surface and reduce the radar backscatter coefficient. This results in dark regions or spots in SAR images. However, other physical phenomena, for example, low-wind areas, areas of wind-shadow near coasts, rain cells, currents, zones of upwelling, biogenic films, internal waves, and oceanic or atmospheric fronts, can also generate dark areas, known as look-alikes, in SAR images (Brekke & Solberg, 2005; Topouzelis, 2008). Another factor which influences the backscatter level and the visibility of slicks on the sea surface is the wind level. Oil slicks are visible only for a limited range of wind speeds (Brekke & Solberg, 2005; Topouzelis, 2008).

Generally speaking, the procedure of detecting oil spills from SAR images can be summarized three steps (Solberg, Storvik, Solberg & Volden, 1999): (1) dark spot detection which identifies all dark spots presented in a SAR image as candidates of potential oil spills; (2) feature extraction which obtains geometric and statistical features for each oil spill candidate, such as area and perimeter and physical behaviour for example mean and variance of backscatter values; and (3) classification which recognizes the oil spills from look-alikes according to the features extracted above. Dark spot detection is a critical and fundamental step as a prelude for further feature extraction and classification of oil spills. Many dark spot detection algorithms have been developed. The commonly used approaches to dark spot detection are so called threshold based algorithms. The thresholds can be simply selected by taking the half of the average Normalized Radar Cross Section (NRCS) of the image (Fiscella, Giancaspro, Nirchio, Pavese & Trivero, 2000), or NRCS minus the standard deviation (Nirchio et al., 2005), or analyzing bimodal histograms (Skϕelv & Wahl, 1993; Manore, Vachon,

* Corresponding author. Tel.: +1 519 8884567x34504; fax: +1 519 7460658.
E-mail address: junli@uwaterloo.ca (J. Li).

0034-4257/$ – see front matter.
doi:10.1016/j.rse.2010.02.013

Bjerkelund, Edel & Ramsay, 1998; Vachon et al., 1998). The adaptive threshold algorithm is proposed by Solberg et al. (1999);Solberg, Dokken and Solberg (2003), in which the threshold is set k dB below the mean value estimated in a moving window and is calculated using a multiscale pyramid approach and a clustering step. The hysteresis thresholding is used by Kanaa et al. (2003) for detecting oil spill in ERS amplitude images. Other techniques used for detecting dark spots include edge detection techniques such as the Laplace of Gaussian (LoG) and Difference of Gaussian (DoG) operators (Chang, Chen, Chen & Chen, 1996; Chen, Chen, Chang & Chen, 1997), wavelet technique (Liu, Peng & Chang, 1997; Wu & Liu, 2003; Derrode & Mercier, 2007), fractal dimension estimation (Benelli & Garzelli, 1999; Marghany, Hashim & Cracknell, 2007), and neural network (Topouzelis, Karathanassi, Pavlakis & Rokos, 2008).

SAR images are highly speckled due to coherent processing (Lee, Jurkevich, Dewaele, Wambacq & Oosterlinck, 1994). The analysis of SAR data is usually required to region and statistics based in order to reduce the speckle effect. Following this idea, a new algorithm for the detection of dark spots from SAR intensity images is studied. Under Bayesian paradigm, the proposed algorithm is based on Poisson marked point process (Stoyan, Kendall & Mecke, 1995) and Reversible Jump Markov chain Monte Carlo (RJMCMC) (Green, 1995). In order to detect dark spots in SAR intensity images, the dark spots are located by a group of random points and their areas are represented by a series of rectangle windows centred at the points. The number of points in the point process is assumed to be random variable which follows a Poisson distribution with fixed mean given by user. In practice, selecting the mean is not very reliable as it depends on the experience of human operators and sometimes is impossible since the ground true is always unknown in advance. The intensities of pixels in and out of the windows are modelled by two strict stationary random fields, respectively. That is, both of them satisfy independent and identical gamma distributions (Lee, Hoppel, Mango & Miller, 1994) but the means for the former are less than that for the latter. Following the Bayesian paradigm, the mathematical form for the posterior distribution is obtained up to a normalizing constant. A RJMCMC algorithm is introduced for simulation from the posterior distribution. And the optimal locations and sizes of dark spots can be obtained by maximum a posteriori (MAP) scheme.

The paper is organized as follows. Section 2 gives the concept of marked point process. Section 3 describes the proposed algorithm. Section 4 shows some results of oil spill detection from RADARSAT-1 images. Section 5 concludes and gives some perspectives.

2. Marked point process

Marked point process models are useful tools to analyze irregularly space data. Generally speaking, a random point process in R^d is a random set in R^d, each realization of which consists of a finite or countable number of points (Stoyan et al., 1995). For simplicity, the following discussion on random point process will be limited on two-dimension case, that is, $d=2$.

When the locations of k random points are independently and uniformly distributed over a domain, a binomial point process can be formed by the k random points. For example, in two dimension case, such a process is formed by k independent points $\boldsymbol{G}=\{(u_j, v_j); j=1,2,\ldots, k, (u_j, v_j)\in D\subset R^2\}$ uniformly distributed on D. Fig. 1 shows a realization of a binomial point process in R^2 (Stoyan et al., 1995).

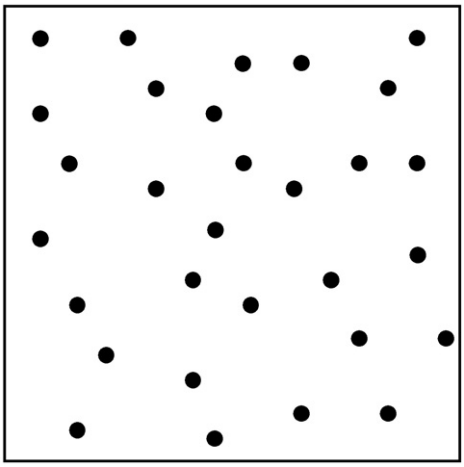

Fig. 1. Realization of a binomial point process in R^2.

A marked point process can be constructed from a random point process by attaching a characteristic (or mark) to each point of the process. Thus, a marked point process on R^2 is a random sequence $\{(u_j, v_j, M_j), j=1, 2, \ldots, k\}$, from which the points (u_j, v_j) together constitute a point process (not mark) in R^2 while the mark M_j corresponding to (u_j, v_j) may have a complicated structure (Schabenberger & Gotway, 2005). They belong to a given space of marks which are assumed to be a Polish space (Stoyan et al., 1995).

Several studies on considering the marked point processes framework for image analysis can be found in the literature. Rue and Hurn (1999) presented an algorithm for locating and identifying an unknown number of objects in an image by combining marked point processes as objects priors and deformable template models. Descombes and Zerubia (2002) showed that marked point processes are more adapted than Markov random field and proposed some applications in remote sensing: road network extraction, building extraction, and image segmentation. Hartvig (2002) presented a marked point process based approach to estimating spatial activation patterns in functional magnetic resonance imaging, in which points are considered as centers of activation and the marks as parameters describing the shape and area of the surrounding cluster. Al-Awadhi, Jennison and Hurn (2004) considered a model for the analysis of confocal fluorescence microscope images of cells in an area of cartilage growth. In their model of the imaging process, the true scene is treated as a realization of marked point process, incorporating this as the high level prior model in a Bayesian analysis. Quartulli and Datcu (2004) proposed a model-based algorithm for the automatic reconstruction of building areas from single-observation meter-resolution SAR intensity data, which is based on the MAP estimation for obtaining optimal scene that is modeled as a set of mutually interacting Poisson marked points describing building objects.

3. Description of proposed algorithm

3.1. Bayesian model for dark spots

Consider a SAR intensity image $\boldsymbol{Z}=\{Z_i=Z(x_i, y_i); i=1, \ldots, n, (x_i, y_i)\in D\}$ where i is the index of pixel, (x_i, y_i) is the location of pixel i, Z_i is a sample of random variable Z at (x_i, y_i) representing the intensity of pixel i, n is the number of pixels in $\boldsymbol{Z}$, and D is the domain of $\boldsymbol{Z}$. Assume that $\boldsymbol{Z}$ contains an unknown but bounded number k of dark spots corresponding to the candidate of oil spills and k has a prior distribution with probability function $p(k)$. The j'th dark spot is modeled by a window W_j with length l_j, width w_j, direction a_j, and centred at pixel $(u_j, v_j)\in D$ called the central point of W_j which is randomly distributed on D with a prior density $p(u_j, v_j)$. Let $\boldsymbol{G}=\{(u_j, v_j); j=1, \ldots, k\}$ and $\boldsymbol{\Phi}=\{(l_j, w_j, a_j); j=1, \ldots, k\}$

be the sets of central points and the geometric parameters of windows, respectively. The Fig. 2 shows the structure. In order to distinguish dark spots from their background, D can be divided into two regions, that is, $D=\{D_d, D_b\}$ where $D_d=\{W_j; j=1,\ldots,k\}$ and $D_b=D\backslash D_d$ correspond to dark spot and sea regions, respectively. In this paper, assume that the intensities of pixels in these regions are characterized by gamma distribution (Lee, Hoppel, et al., 1994b), that is,

$$p(Z_i)=\begin{cases}\dfrac{Z_i^{\alpha_j-1}}{\beta_j^{\alpha_j}\Gamma\left(\alpha_j\right)}e^{-\dfrac{Z_i}{\beta_j}} & \text{if } (x_i,y_i)\in W_j\\ \dfrac{Z_i^{\alpha_0-1}}{\beta_0^{\alpha_0}\Gamma(\alpha_0)}e^{-\dfrac{Z_i}{\beta_0}} & \text{if } (x_i,y_i)\in D_b\end{cases} \tag{1}$$

where $\Gamma(\cdot)$ is the gamma function, α_j and β_j are the shape and scale parameters of gamma distribution for the intensities of the pixels in W_j, α_0 and β_0 are the shape and scale parameters of gamma distribution for the intensities of the pixels in D_b. Under the above assumption, the dark spots can be identified by the constrain on the distribution parameters, that is,

$$\alpha_0\beta_0>\alpha_j\beta_j \quad \text{for all } j=1,\ldots,k \tag{2}$$

Assume that all intensities are independent. Then the joint distributions of intensities in W_j and D_b can be expressed as follows

$$p\left(\mathbf{Z}_{Wj}\,|\,\boldsymbol{\theta}_j,W_j\right)=\prod_{(x_i,y_i)\in W_j}\frac{Z_i^{\alpha_j-1}}{\beta_j^{\alpha_j}\Gamma\left(\alpha_j\right)}e^{-\frac{Z_i}{\beta_j}} \tag{3}$$

$$p(\mathbf{Z}_{Db}\,|\,\boldsymbol{\theta}_0,D_b)=\prod_{(x_i,y_i)\in D_b}\frac{Z_i^{\alpha_0-1}}{\beta_0^{\alpha_0}\Gamma(\alpha_0)}e^{-\frac{Z_i}{\beta_0}} \tag{4}$$

where $\boldsymbol{Z}_{Wj}=\{Z_i;\ (x_i,\ y_i)\in W_j\}$, $\boldsymbol{Z}_{Db}=\{Z_i;\ (x_i,\ y_i)\in D_b\}$, $\boldsymbol{\theta}_j=(\alpha_j,\ \beta_j)$ and $\boldsymbol{\theta}_0=(\alpha_0,\ \beta_0)$. Let $\boldsymbol{\theta}=(\boldsymbol{\theta}_{j'}=(\alpha_{j'},\ \beta_{j'});\ j'=0,\ 1,\ \ldots,\ k)$ be the distribution parameter vector. The likelihood can be defined as

$$p(\mathbf{Z}\,|\,\boldsymbol{\theta},\mathbf{G},\Phi,k)=p(\mathbf{Z}_{Db}\,|\,\boldsymbol{\theta}_0,D_b)\times\prod_{j\in\{1,\ldots,k\}}p\left(\mathbf{Z}_{Wj}\,|\,\boldsymbol{\theta}_j,W_j\right) \tag{5}$$

In order to detect dark spots, the posterior distribution of distribution parameter vector $\boldsymbol{\theta}$, geometric parameter vector $\boldsymbol{\Phi}$, the position vector $\boldsymbol{G}$ as well as the number of windows k is primarily considered. By Bayesian paradigm, the posterior distribution conditional on $\boldsymbol{Z}$ can be written as,

$$p(\boldsymbol{\theta},\mathbf{G},\Phi,k\,|\,\mathbf{Z})\propto p(\mathbf{Z}\,|\,\boldsymbol{\theta},\mathbf{G},\Phi,k)p(\boldsymbol{\theta})p(\mathbf{G}\,|\,k)p(\Phi\,|\,k)p(k) \tag{6}$$

3.2. Prior distributions and the likelihood

The prior distributions of shape and scale parameters α and parameter β are assumed to be normal distribution, but with different means and standard deviations for dark spot class and background class, that is, $\alpha_{j=1,\ldots,k}\sim N(\mu_\alpha,\sigma_\alpha^2)$, $\beta_{j=1,\ldots,k}\sim N(\mu_\beta,\sigma_\beta^2)$, $\alpha_0\sim N(\mu_{\alpha0},\sigma_{\alpha0}^2)$, $\beta_0\sim N(\mu_{\beta0},\sigma_{\beta0}^2)$,

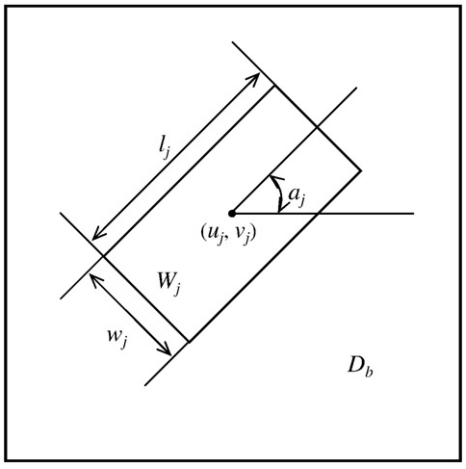

Fig. 2. The Structure of window with length l_j, width w_j and direction a_j centered at points (u_j, v_j).

respectively. The independent, weakly informative normal distributions assumed for prior structures are maintained for simplicity. Their probability density functions can be expressed as

$$p\left(\alpha_j\right) = \frac{1}{\sqrt{2\pi}\sigma_\alpha} e^{-\frac{\left(\alpha_j-\mu_\alpha\right)^2}{2\sigma_\alpha^2}} \tag{7}$$

$$p\left(\beta_j\right) = \frac{1}{\sqrt{2\pi}\sigma_\beta} e^{-\frac{\left(\beta_j-\mu_\beta\right)^2}{2\sigma_\beta^2}} \tag{8}$$

$$p(\alpha_0) = \frac{1}{\sqrt{2\pi}\sigma_{\alpha 0}} e^{-\frac{(\alpha_0-\mu_{\alpha 0})^2}{2\sigma_{\alpha 0}^2}} \tag{9}$$

$$p(\beta_0) = \frac{1}{\sqrt{2\pi}\sigma_{\beta 0}} e^{-\frac{\left(\beta_0-\mu_{\beta 0}\right)^2}{2\sigma_{\beta 0}^2}} \tag{10}$$

Assume that all distribution parameters are independent each other, the prior distribution of $\boldsymbol{\theta} = \{\alpha_0, \alpha_1, \ldots, \alpha_k, \beta_0, \beta_1, \ldots, \beta_k\}$ can be written as follows

$$p(\boldsymbol{\theta}|k) = \frac{1}{2\pi\sigma_{\alpha 0}\sigma_{\beta 0}} e^{-\frac{(\alpha_0-\mu_{\alpha 0})^2}{2\sigma_{\alpha 0}^2}} e^{-\frac{\left(\beta_0-\mu_{\beta 0}\right)^2}{2\sigma_{\beta 0}^2}} \prod_{j=1}^{k} \frac{1}{2\pi\sigma_\alpha\sigma_\beta} e^{-\frac{\left(\alpha_j-\mu_\alpha\right)^2}{2\sigma_\alpha^2}} e^{-\frac{\left(\beta_j-\mu_\beta\right)^2}{2\sigma_\beta^2}} \tag{11}$$

Assume that the central points are uniformly distributed on the image domain D, then the prior distribution of $\boldsymbol{G}$ can be written as

$$p(\mathbf{G}|k) = \left(\frac{1}{|D|}\right)^k \tag{12}$$

where $|D|$ is the area of image domain D.

The lengths and widths of windows are assumed to be normal distributions, that is, $l_j \sim N(\mu_l, \sigma_l^2)$, $w_j \sim N(\mu_w, \sigma_w^2)$, while the directions of windows are the uniform distribution on $[-\pi/2, \pi/2]$, that is, $a_j \sim U(-\pi/2, \pi/2)$. Assume that the geometric parameters are independent. As a result, the prior distribution of $\boldsymbol{\Phi}$ can be written as

$$p(\Phi|k) = \prod_{j=1}^{k} \frac{1}{2\pi^2\sigma_l\sigma_w} e^{-\frac{\left(l_j-\mu_l\right)^2}{2\sigma_l^2}} e^{-\frac{\left(w_j-\mu_w\right)^2}{2\sigma_w^2}} \tag{13}$$

The number of windows k is assumed to have a prior truncated Poisson distribution with mean λ (Green, 1995)

$$p(k) = \frac{\lambda^k e^{-\lambda}}{k!} \tag{14}$$

where the k is truncated with minimum $k=1$ and maximum $k=k_{\max}$ where $k_{\max}$ is set by user. k_m has a maximum around $\min\{n_1/\min(\mu_l, \mu_w), n_2/\min(\mu_l, \mu_w)\}$ where n_1 and n_2 are the dimensions of an image.

The posterior distribution in Eq. (6) can be rewritten as

$$p(\boldsymbol{\theta}, \mathbf{G}, \Phi, k|\mathbf{Z}) = \prod_{(x_i,y_i)\in D_b} Z_i^{\alpha_0-1} \frac{e^{-Z_i/\beta_0}}{\beta_0^{\alpha_0}\Gamma(\alpha_0)} \times \prod_{j=1}^{k} \prod_{(x_i,y_i)\in W_j} Z_i^{\alpha_j-1} \frac{e^{-Z_i/\beta_j}}{\beta_j^{\alpha_j}\Gamma\left(\alpha_j\right)} \times \frac{1}{2\pi\sigma_{\alpha 0}\sigma_{\beta 0}} e^{-\frac{(\alpha_0-\mu_{\alpha 0})^2}{2\sigma_{\alpha 0}^2}} e^{-\frac{\left(\beta_0-\mu_{\beta 0}\right)^2}{2\sigma_{\beta 0}^2}} \tag{15}$$

$$\prod_{j=1}^{k} \frac{1}{2\pi\sigma_\alpha\sigma_\beta} e^{-\frac{\left(\alpha_j-\mu_\alpha\right)^2}{2\sigma_\alpha^2}} e^{-\frac{\left(\beta_j-\mu_\beta\right)^2}{2\sigma_\beta^2}} \times \prod_{j=1}^{k} \frac{1}{2\pi^2\sigma_l\sigma_w} e^{-\frac{\left(l_j-\mu_l\right)^2}{2\sigma_l^2}} e^{-\frac{\left(w_j-\mu_w\right)^2}{2\sigma_w^2}} \times \left(\frac{1}{|D|}\right)^k \times \frac{\lambda^k e^{-\lambda}}{k!}$$

3.3. Estimation and simulation algorithms

In order to detect dark spots from a SAR image, it is necessary to simulate from the posterior distribution defined in Eq. (15) and estimate parameters. Let $\boldsymbol{\theta} = (\boldsymbol{\theta}, \boldsymbol{G}, \boldsymbol{\Phi}, k)$ be a parameter vector. It is worthy to note when k is varied, the dimension of the parameter vector $\boldsymbol{\theta}$ is varied. In this paper, the Metropolis–Hastings (Gilks, Richardson & Spiegelhalter, 1996) and RJMCMC algorithms (Green, 1995) are used to simulate dependent samples from the posterior distribution of $\boldsymbol{\theta}$ while the parameter space is variable during sampling. According to Green (1995), a new candidate $\boldsymbol{\theta}^*$ for $\boldsymbol{\theta}$ is proposed at each iteration by an invertible deterministic function $\boldsymbol{\theta}^* = \boldsymbol{\theta}^*(\boldsymbol{\theta}, \boldsymbol{s})$ (assume that the dimension of $\boldsymbol{\theta}^*$ is higher

than that of $\boldsymbol{\theta}$), where $\boldsymbol{s}$ is a random vector defined for accomplishing a transition from $(\boldsymbol{\theta}, \boldsymbol{s})$ to $\boldsymbol{\theta}^*$ with the dimension satisfying the dimension matching condition, that is, $|\boldsymbol{\theta}|+|\boldsymbol{s}|=|\boldsymbol{\theta}^*|$ (Green, 1995). The appropriate acceptance probability for the proposed transition from $\boldsymbol{\theta}$ to $\boldsymbol{\theta}^*$ is given by

$$\alpha(\boldsymbol{\theta}, \boldsymbol{\theta}^*) = \min\left\{1, \frac{p(\boldsymbol{\theta}^*|\mathbf{Z})r(\boldsymbol{\theta}^*)}{p(\boldsymbol{\theta}|\mathbf{Z})r(\boldsymbol{\theta})q(\boldsymbol{s})}\left|\frac{\partial\boldsymbol{\theta}^*}{\partial(\boldsymbol{\theta}, \boldsymbol{s})}\right|\right\} \tag{16}$$

where $q(\boldsymbol{s})$ is the density function of $\boldsymbol{s}$ and $r(\boldsymbol{\theta}^*)$ and $r(\boldsymbol{\theta})$ are the probabilities of a given move type in the states $\boldsymbol{\theta}^*$ and $\boldsymbol{\theta}$, respectively. The joint probability density measures $r(\boldsymbol{\theta}^*)$ and $r(\boldsymbol{\theta})$ ensure that 'detailed balance' is maintained with any change of dimension in the state space variable (Green, 1995). The Jacobian $|\partial\boldsymbol{\theta}^*/\partial(\boldsymbol{\theta}, \boldsymbol{s})|$ is due to the change of variable from $(\boldsymbol{\theta}, \boldsymbol{s})$ to $\boldsymbol{\theta}^*$. If a type of move is proposed that does not involve a change in dimension of the random variable $\boldsymbol{\theta}$, then Eq. (16) reduces to usual Metropolis–Hastings acceptance probability.

In developing a RJMCMC sampler for marked point process based oil-spill detection, it is necessary to design different types of move between the parameter subspaces at each iteration, in order to traverse freely across the combined parameters space of $\boldsymbol{\theta}$. The move types designed in this paper include: (1) updating the geometric parameters of windows: the length, width and direction; (2) updating gamma distribution parameters; (3) updating the positions of central points; and (4) birth or death of windows.

3.3.1. Move 1: updating the geometric parameters of windows

The geometric parameters can be rearranged as $\boldsymbol{\Phi}=\{(l_j, w_j, a_j); j=1, \ldots, k\}=\{\Phi_{j'}; j'=1, \ldots, 3k\}$. At t'th iteration the proposal $\Phi_{j'}^*$ is drawn from a Gaussian distribution with mean $\Phi_{j'}^{(t-1)}$ and variance ε which is equal to ε_l, ε_w, and ε_a as $\Phi_{j'}=l_j, w_j, a_j$, respectively. That is, $\Phi_{j'}^* \sim N(\Phi_{j'}^{(t-1)}, \varepsilon)$. Fig. 3 shows the change of window structures in terms of its length l_j, width w_j and direction a_j, respectively.

The acceptance probability for the proposal $\Phi_{j'}^*$ is given by

$$r_l = \min\left\{1, \frac{p\left(\mathbf{Z}_{Wj^*}\right)p(\mathbf{Z}_{Db^*})p\left(l_j^*\right)}{p\left(\mathbf{Z}_{Wj}\right)p(\mathbf{Z}_{Db})p\left(l_j\right)}\right\} = \begin{cases} \min\left\{1, \dfrac{\prod_{(x_i,y_i)\in W_j^*\setminus W_j} Z_i^{\alpha_j-1}\dfrac{e^{-Z_i/\beta_j}}{\beta_j^{\alpha_j}\Gamma\left(\alpha_j\right)}}{\prod_{(x_i,y_i)\in W_j^*\setminus W_j} Z_i^{\alpha_0-1}\dfrac{e^{-Z_i/\beta_0}}{\beta_0^{\alpha_0}\Gamma(\alpha_0)}} \times \dfrac{e^{-\frac{\left(l_j^*-\mu_l\right)^2}{2\sigma_l^2}}}{e^{-\frac{\left(l_j-\mu_l\right)^2}{2\sigma_l^2}}}\right\}, & \text{if } l_j^* > l_j \\ \min\left\{1, \dfrac{\prod_{(x_i,y_i)\in W_j\setminus W_j^*} Z_i^{\alpha_0-1}\dfrac{e^{-Z_i/\beta_0}}{\beta_0^{\alpha_0}\Gamma(\alpha_0)}}{\prod_{(x_i,y_i)\in W_j^*\setminus W_j} Z_i^{\alpha_j-1}\dfrac{e^{-Z_i/\beta_j}}{\beta_j^{\alpha_j}\Gamma\left(\alpha_j\right)}} \times \dfrac{e^{-\frac{\left(l_j^*-\mu_l\right)^2}{2\sigma_l^2}}}{e^{-\frac{\left(l_j-\mu_l\right)^2}{2\sigma_l^2}}}\right\}, & \text{if } l_j^* < l_j \end{cases} \tag{17}$$

$$r_w = \min\left\{1, \frac{p\left(\mathbf{Z}_{Wj*}\right)p(\mathbf{Z}_{Db*})p\left(w_j^*\right)}{p\left(\mathbf{Z}_{Wj}\right)p(\mathbf{Z}_{Db})p\left(w_j\right)}\right\} = \begin{cases} \min\left\{1, \dfrac{\prod_{(x_i,y_i)\in W_j^*\setminus W_j} Z_i^{\alpha_j-1}\dfrac{e^{-Z_i/\beta_j}}{\beta_j^{\alpha_j}\Gamma\left(\alpha_j\right)}}{\prod_{(x_i,y_i)\in W_j^*\setminus W_j} Z_i^{\alpha_0-1}\dfrac{e^{-Z_i/\beta_0}}{\beta_0^{\alpha_0}\Gamma(\alpha_0)}} \times \dfrac{e^{-\frac{\left(w_j^*-\mu_l\right)^2}{2\sigma_l^2}}}{e^{-\frac{\left(w_j-\mu_l\right)^2}{2\sigma_l^2}}}\right\}, & \text{if } w_j^* > w_j \\ \min\left\{1, \dfrac{\prod_{(x_i,y_i)\in W_j\setminus W_j^*} Z_i^{\alpha_0-1}\dfrac{e^{-Z_i/\beta_0}}{\beta_0^{\alpha_0}\Gamma(\alpha_0)}}{\prod_{(x_i,y_i)\in W_j^*\setminus W_j} Z_i^{\alpha_j-1}\dfrac{e^{-Z_i/\beta_j}}{\beta_j^{\alpha_j}\Gamma\left(\alpha_j\right)}} \times \dfrac{e^{-\frac{\left(w_j^*-\mu_l\right)^2}{2\sigma_l^2}}}{e^{-\frac{\left(w_j-\mu_l\right)^2}{2\sigma_l^2}}}\right\}, & \text{if } w_j^* < w_j \end{cases} \tag{18}$$

$$r_a = \min\left\{1, \frac{p\left(\mathbf{Z}_{Wj_*}\right)p(\mathbf{Z}_{Db*})p\left(a_j^*\right)}{p\left(\mathbf{Z}_{Wj}\right)p(\mathbf{Z}_{Db})p\left(a_j\right)}\right\} \tag{19}$$

$$= \min\left\{1, \frac{\prod_{(x_i,y_i)\in W_j^*\setminus W_j} Z_i^{\alpha_j-1}\dfrac{e^{-Z_i/\beta_j}}{\beta_j^{\alpha_j}\Gamma\left(\alpha_j\right)}}{\prod_{(x_i,y_i)\in W_j^*\setminus W_j} Z_i^{\alpha_0-1}\dfrac{e^{-Z_i/\beta_0}}{\beta_0^{\alpha_0}\Gamma(\alpha_0)}} \times \frac{\prod_{(x_i,y_i)\in W_j\setminus W_j^*} Z_i^{\alpha_0-1}\dfrac{e^{-Z_i/\beta_0}}{\beta_0^{\alpha_0}\Gamma(\alpha_0)}}{\prod_{(x_i,y_i)\in W_j^*\setminus W_j} Z_i^{\alpha_j-1}\dfrac{e^{-Z_i/\beta_j}}{\beta_j^{\alpha_j}\Gamma\left(\alpha_j\right)}}\right\}$$

where W_j^* and W_j are the windows constructed by (l_j^*, w_j^*, a_j^*) and (l_j, w_j, a_j), respectively.

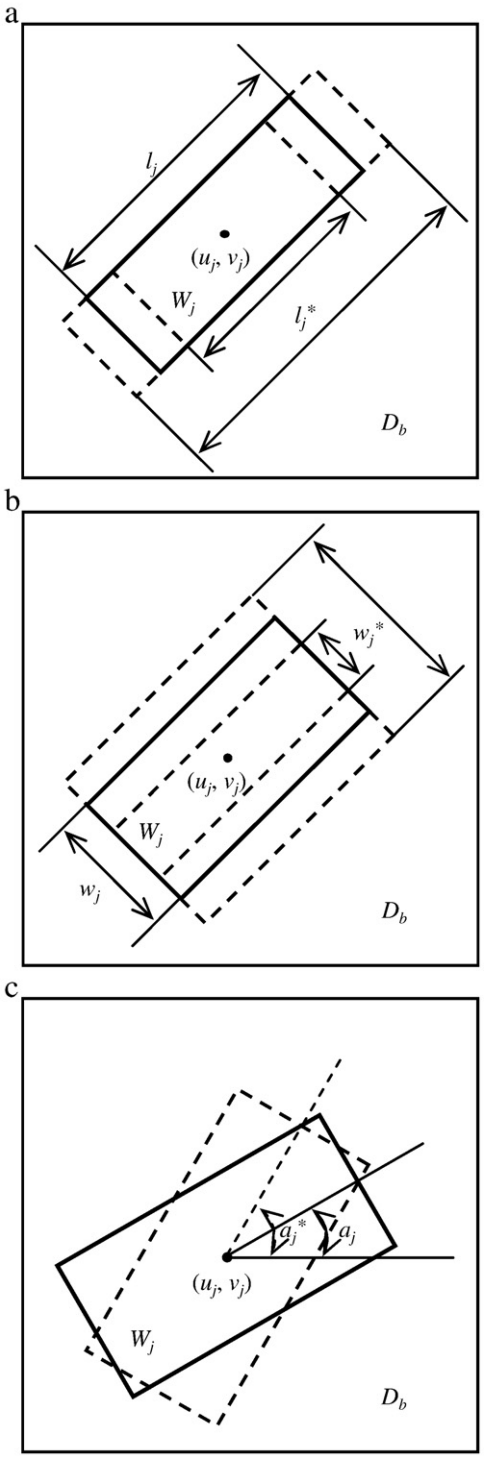

Fig. 3. The change of window in terms of length l_j, width w_j and direction a_j.

3.3.2. Move 2: updating gamma distribution parameters

Rewrite the distribution parameter vector as $\boldsymbol{\theta} = \{\boldsymbol{\theta}_{j'}, j' = 0, 1, \ldots, k\}$ where $\boldsymbol{\theta}_{j'} = (\alpha_{j'}, \beta_{j'})$. Assume that the probability distributions for the proposal $\alpha_{j'}^*$ and $\beta_{j'}^*$ at t'th iteration are Gaussian distributions with means $\alpha_{j'}^{(t-1)}$ and $\beta_{j'}^{(t-1)}$, and standard difference ε_α and ε_β, that is, $\alpha_{j'}^* \sim N(\alpha_{j'}^{(t-1)}, \varepsilon_\alpha)$ and $\beta_{j'}^* \sim N(\beta_{j'}^{(t-1)}, \varepsilon_\beta)$. The acceptance probability for the proposal $\alpha_{j'}^*$ and $\beta_{j'}^*$ can be obtained as

$$r_{\alpha,\beta} = \min\left\{1, \frac{\prod_{(x_i,y_i)\in W_j} p\left(Z_i|\boldsymbol{\theta}_j^*\right) \times p\left(\boldsymbol{\theta}_j^*\right)}{\prod_{(x_i,y_j)\in W_j} p\left(Z_i|\boldsymbol{\theta}_j\right) \times p\left(\boldsymbol{\theta}_j\right)}\right\} \tag{20}$$

$$r_{\alpha_0,\beta_0} = \min\left\{1, \frac{\prod_{(x_i,y_i)\in D_b} p\left(Z_i|\theta_0^*\right)\times p\left(\theta_0^*\right)}{\prod_{(x_i,y_j)\in B_b} p(Z_i|\theta_0)\times p(\theta_0)}\right\} \tag{21}$$

3.3.3. Move 3: moving the position of central points

At t'th iteration, one of central points in $\boldsymbol{G}=\{(u_j^{(t-1)}, v_j^{(t-1)}), j=1,\ldots,k\}$ is drawn at random, say $(u_j^{(t-1)}, v_j^{(t-1)})$. A proposed position is (u_j^*, v_j^*) by drawing uniformly in the window W_j. The new position of the central point gives rise to the local changes of W_j to W_j^*. Fig. 4 shows the example for the change.

The acceptance probability for the move turns out to be

$$r_c = \min\left\{1, \frac{p\left(\mathbf{Z}_{Wj*}\right)p(\mathbf{Z}_{Db*})p\left(u_j^*, v_j^*\right)}{p\left(\mathbf{Z}_{Wj}\right)p(\mathbf{Z}_{Db})p\left(u_j, u_{vj}\right)}\right\} \tag{22}$$

$$= \min\left\{1, \frac{\prod_{(x_i,y_i)\in W_j^*\setminus W_j}\beta_j^{\alpha_j}\exp\left(-\frac{Z_i}{\beta_j}\right)\times\prod_{(x_i,y_i)\in W_j\setminus W_j^*}\beta_0^{\alpha_0}\exp\left(-\frac{Z_i}{\beta_0}\right)}{\prod_{(x_i,y_i)\in W_j^*\setminus W_j}\beta_0^{\alpha_0}\exp\left(-\frac{Z_i}{\beta_0}\right)\times\prod_{(x_i,y_i)\in W_j\setminus W_j^*}\beta_j^{\alpha_j}\exp\left(-\frac{Z_i}{\beta_j}\right)}\right\}$$

3.3.4. Move 4: birth or death of generating points

Suppose that the current number of central points is k and let the probabilities of proposing a birth or death operation be b_k or d_k, respectively. Consider a birth operation which increases the number of central points from k to $k+1$ and assume that the new central point is labelled with $k+1$ and its location (u_{k+1}, v_{k+1}) is drawn uniformly from $D\backslash D_d$. Let the window induced by (u_{k+1}, v_{k+1}) be W_{k+1}. The proposal position vector becomes $\boldsymbol{G}^*=\{(u_1, v_1), \ldots, (u_k, v_k), (u_{k+1}, v_{k+1})\}$. As a result, the parameter vector for the birth operation becomes $\boldsymbol{\Theta}^*=(\boldsymbol{\theta}, \boldsymbol{G}^*, \boldsymbol{\Phi}\, k+1)$. The acceptance probability for the birth can be written as

$$r_b(\boldsymbol{\Theta}, \boldsymbol{\Theta}^*) = \min\{1, R_b\} \tag{23}$$

where

$$R_b = \frac{p(\mathbf{Z}|\boldsymbol{\theta}, \mathbf{G}^*, k+1)p(k+1)p(\mathbf{G}^*|k+1)r_{b_k}(\boldsymbol{\Theta}^*)}{p(\mathbf{Z}|\boldsymbol{\theta}, \mathbf{G}, k)p(k)p(\mathbf{G}|k)r_{d_{k+1}}(\boldsymbol{\Theta})q(\mathbf{s})}\frac{\partial(\boldsymbol{\Theta}^*)}{\partial(\boldsymbol{\Theta}, \mathbf{s})} \tag{24}$$

where $r_{bk}=b_k$, $r_{dk+1}=d_{k+1}/(k+1)$, $\boldsymbol{s}=(u_{k+1}, v_{k+1})$ and other terms in Eq. (24) can be expressed as follows

$$\frac{p(\mathbf{Z}|\boldsymbol{\theta}, \mathbf{G}^*, \Phi, k+1)}{p(\mathbf{Z}|\boldsymbol{\theta}, \mathbf{G}, \Phi, k)} = \frac{\prod_{(x_i,y_i)\in W_{k+1}}\beta_{k+1}^{\alpha_{k+1}}\exp\left(-\frac{Z_i}{\beta_{k+1}}\right)}{\prod_{(x_i,y_i)\in W_{k+1}}\beta_0^{\alpha_0}\exp\left(-\frac{Z_i}{\beta_0}\right)} \tag{25}$$

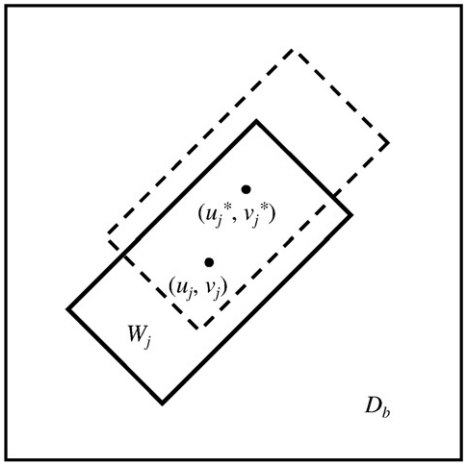

Fig. 4. The change of windows by moving central point.

where α_{k+1} and β_{k+1} are drawn from their prior distribution functions, respectively.

$$\frac{p(k+1)}{p(k)} = \frac{\lambda}{k+1} \tag{26}$$

$$\left|\frac{\partial(\Theta^*)}{\partial(\Theta,\mathbf{s})}\right| = 1 \tag{27}$$

$$q(\mathbf{s}) = \frac{1}{|W_{k+1}|} \tag{28}$$

where $|W_{k+1}|$ is the area of the window W_{k+1}. The acceptance probability for a death of central point is

$$r_d(\Theta,\Theta^*) = \min\{1, R_d\}, \text{and } R_d = R_b^{-1} \tag{29}$$

For any given proposal with acceptance probability r, it is accepted if and only if $r \geq \xi$, where ξ is drawn from [0, 1] uniformly, that is, $\xi \sim U(0,1)$.

Assume that a set of approximate and dependent samples $\{\boldsymbol{\theta}^{(t)}, t = 1, \ldots, T\}$, where T is the number of predefined iterations, is drawn from the joint posterior density $p(\boldsymbol{\theta}|\boldsymbol{Z})$ by the RJMCMC algorithm. The MAP estimation is used to obtain optimal parameters defined in the joint posterior distribution. The optimal estimation $\boldsymbol{\Phi}_{\text{MAP}}$ under MAP estimate can be written as

$$\boldsymbol{\Theta}_{\text{MAP}} = \arg\max\{p(\boldsymbol{\theta}, \mathbf{G}, \Phi, k|\mathbf{Z})\} \tag{30}$$

4. Experiment and results

The proposed algorithm is applied to SAR intensity images containing oil spills indicated by human analyst. Fig. 5 shows four-look Radarsat-1 SAR intensity images with size 512×512 pixels.

Table 1 lists the constants used in the proposed algorithm for the experiment where λ is the mean of Poisson distribution for the number of dark spots, which is set as 3 to encourage a low number of windows since oil spills are fewer. μ_l (μ_w) and σ_l (σ_w) are the mean and standard deviation of length (width) of window. μ_α ($\mu_{\alpha 0}$) and σ_α

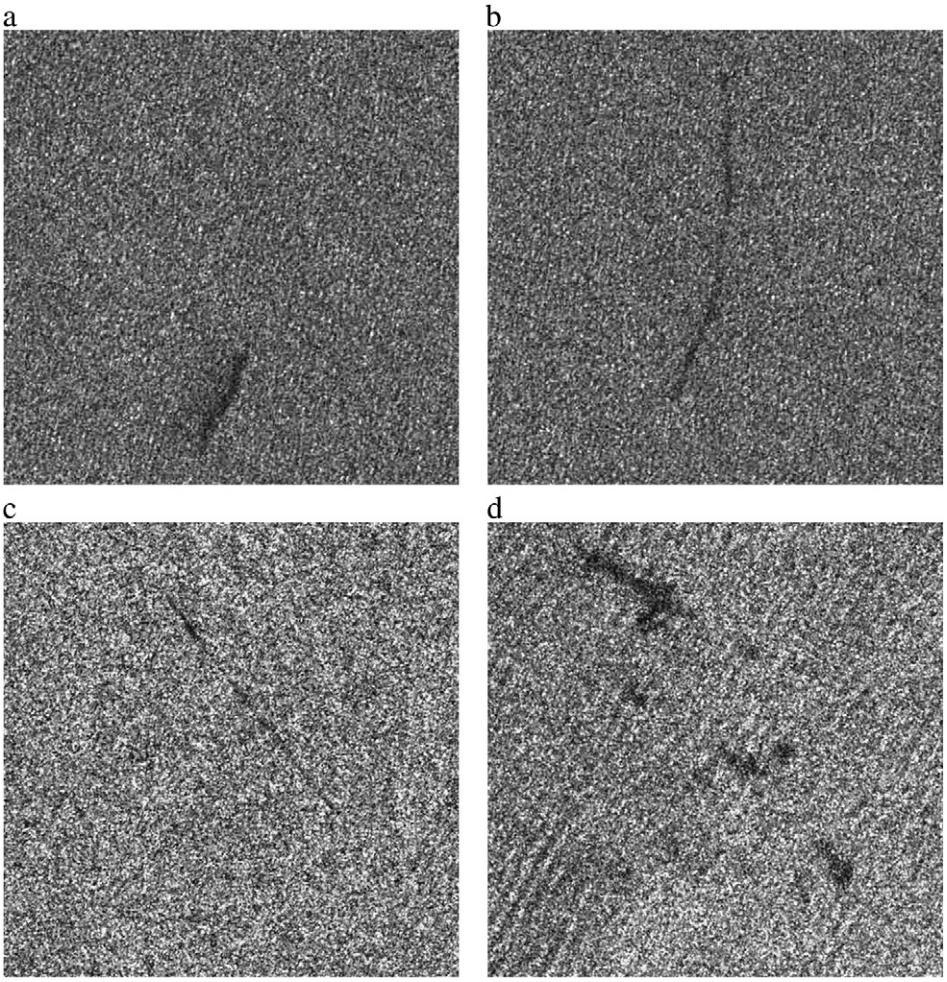

Fig. 5. The Radarsat-1 SAR intensity images.

Table 1
The constants.

λ	μ_l, μ_w	σ_l, σ_w	μ_α, $\mu_{\alpha 0}$	σ_α	μ_β	σ_β
3	50	10	4	0.5	16	2
$\mu_{\beta 0}$	$\varepsilon_{l,\,w}$	ε_a	ε_α	ε_β	T_m	
32	2	$\pi/36$	0.25	1	10000	

($\sigma_{\alpha 0}$) are the mean and standard deviation of the shape parameter of the gamma distributions defined for the dark spots and their background. For a multi-look SAR intensity image in which the intensities of pixels are characterized by gamma distribution, the shape parameter α is equal to the number of its looks. In this paper, since the shape parameters α's are considered as random variables, the values μ_α and $\mu_{\alpha 0}$ are set as the number of looks. For a gamma distribution with shape parameter α and scale parameter β, the product of the two parameters $\alpha \times \beta$ is equal to its mean. Then assume the value $\mu_{\alpha 0} \times \mu_{\beta 0}$ is taken $128 = 256/2$ (i.e. the midpoint of 256 gray levels) since the pixel intensities in a gray-scale image vary in the range 0–255. The constants $\varepsilon_{l,w,a,\alpha,\beta}$ are the proposal variances for l, w, a, α, α_0, β and β_0, respectively, which affect the sampling and convergence of the algorithm under the MCMC scheme (Dryden, Scarr & Taylor, 2003). Though Besag, Green, Higdon and Mengersen (1995) suggested, through their experience, choosing the proposal variances so that the acceptance probability lies in the interval (30–70%). However we have found that the proposal variances causing the acceptance probability around 30% still make the algorithm work well.

Table 2
Estimated parameters.

Image	Window	l (pixel)	w (pixel)	a(°)	u (pixel)	v (pixel)	α	β
a	W_1	64	28	−59.1	235	428	3.47	12.32
	W_2	59	17	−67.4	266	375	3.85	11.90
	W_3	66	18	−52.2	203	431	3.79	11.82
	W_4	49	7	65.7	388	133	3.86	12.07
b	W_1	157	45	−74.7	248	334	3.87	15.33
	W_2	162	27	−87.7	273	125	3.43	13.94
c	W_1	91	12	59.1	203	107	4.07	11.28
	W_2	129	8	51.1	302	238	4.10	13.08
d	W_1	27	31	10.2	396	392	4.21	13.62
	W_2	58	39	−83.4	187	96	4.42	13.35
	W_3	51	22	11.7	290	274	4.16	16.95
	W_4	28	25	13.9	166	194	4.00	15.34
	W_5	65	20	24.5	140	55	4.14	14.00
	W_6	19	55	−33.6	340	271	3.41	16.83

The constant T_m is the maximum iterations of the algorithm. Usually, it depends on the complexity of the scene revealed in a SAR image and requirement of segmentation accuracy. The T_m used in this experiment is uninformative and larger than practically used ones, in order to show the convergence of the proposed algorithm.

The numbers of initial window are drawn from the Poisson distribution with the mean 3. From our experience the number have no significant impact on the final results. The geometric parameters of the initial window are drawn from their distributions. The initial gamma distribution parameters are also drawn from their distributions.

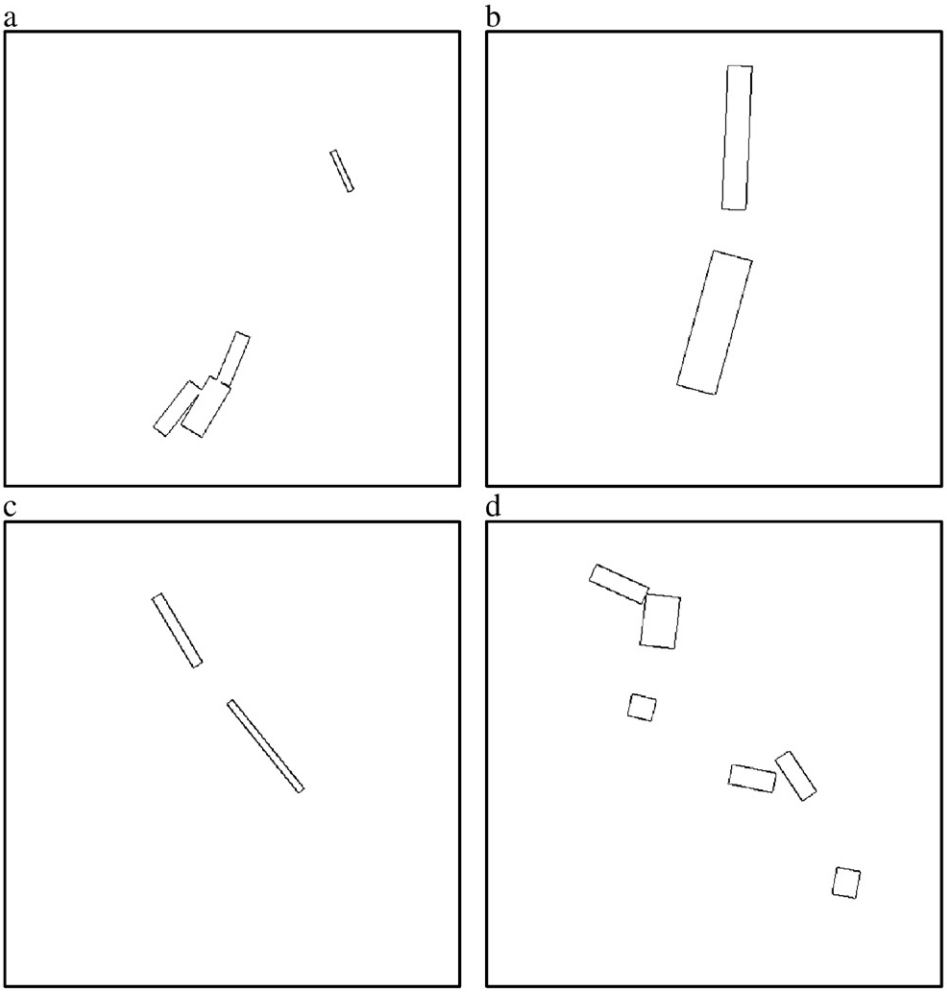

Fig. 6. The outlines of detected windows for the candidates of oil spills.

Table 3
Acceptance rates.

Image	r_l (%)	r_w (%)	r_a (%)	r_c (%)	r_α (%)	r_β (%)	r_b (%)	r_d (%)
a	9.13	14.87	2.25	29.75	70.47	0.49	0.1	0.02
b	23.43	22.49	4.21	29.81	71.25	1.36	1.91	1.95
c	20.97	2.95	1.13	29.04	84.5	0.23	0.01	0.05
d	16.44	17.68	5.13	28.79	91.84	1.05	0.54	0.61

Fig. 6 gives the distribution of final windows after 10,000 iterations, which correspond to the detected dark spots. The numbers of the detected dark spots are 4, 2, 2 and 6 for testing images (a)–(d), respectively.

Table 2 gives the estimated parameters for windows including their lengths, widths, directions, locations of central point and the gamma distribution parameters. The unit of geometric parameters l, w, u, v is pixel.

Table 3 lists the acceptance rate for each type of moves, where r_l, r_w, r_a, r_c, r_α, r_β, r_b and r_d are the acceptance rates of moves for updating length, width, direction, central point of window, shape parameter, scale parameter, moving central point, birth and death of windows, respectively.

Fig. 7 shows the acceptances of proposals (indicated by the value 1) during 10,000 iterations for the SAR image shown in Fig. 5(c). From Fig. 7 (g)–(h) and Table 3, it can be observed that the operations of birth and dead of central point have the minimum acceptance rate and their acceptances are happened within first 6000 iterations. The phenomenon implies that the proposed algorithm can quickly decided the numbers of windows which represent the candidates of oil spills. Since the computation burdens for both of the two moves are very heavy, it is necessary to find a more efficient way to control them, though they have lowest acceptance rates. By contrast, the operation of updating the shape parameter α has the maximum acceptance rate, which is caused by the small ε_α. The more acceptances for moving central points can be explained that the algorithm needs much more changes on the locations of windows to fit the details of dark spots. The updating length of windows operates throughout all iterations, though with middle acceptance rates.

In order to evaluate the accuracy of the proposed algorithm for the detection of dark spots visually, the detected windows (in black) are

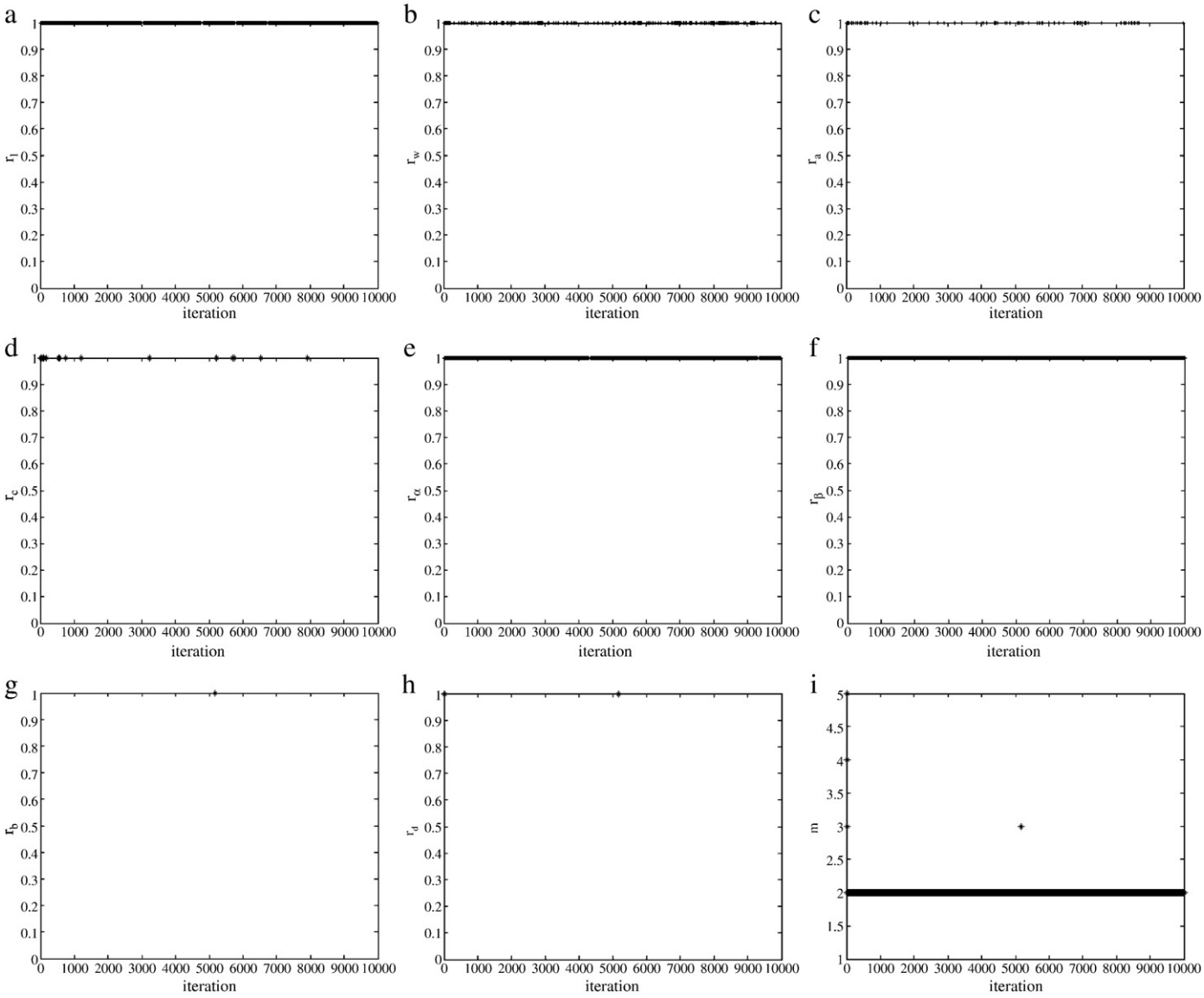

Fig. 7. The acceptance rates (a)–(g) and the change of the number of windows (i) during iterations.

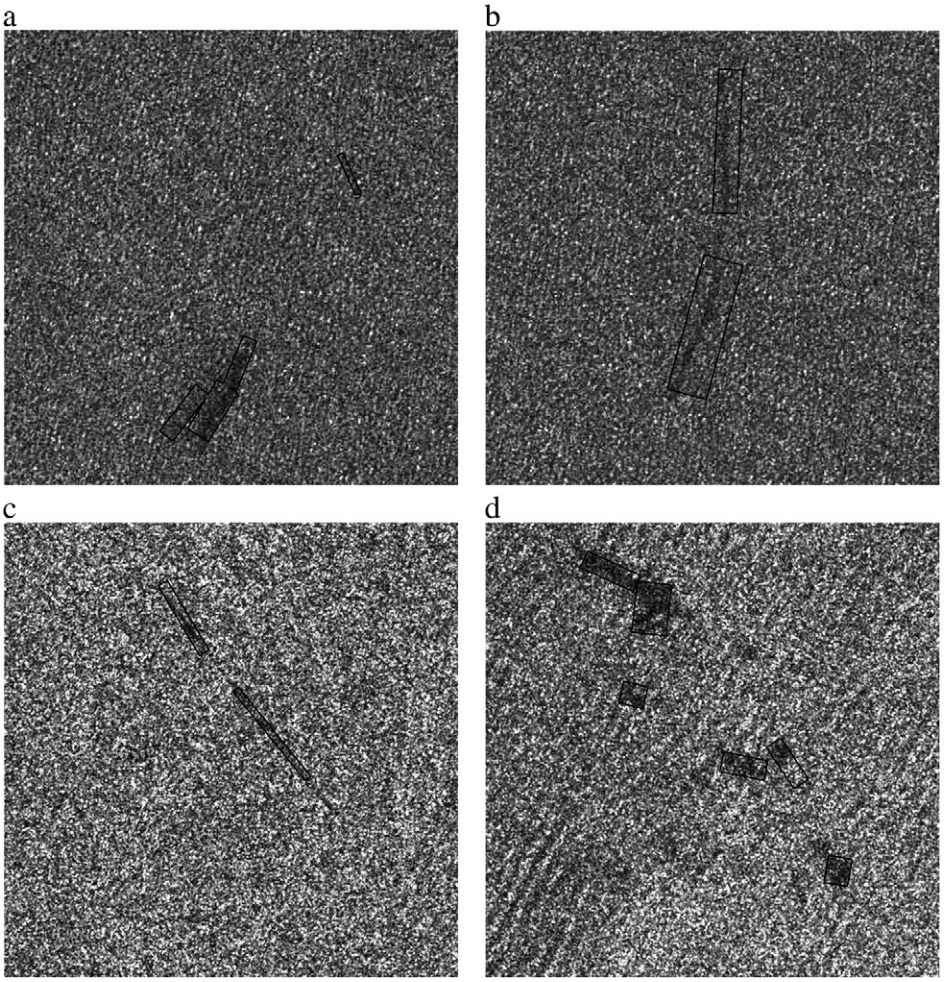

Fig. 8. The overlaying of detected dark spots on the test SAR images.

overlaid on the SAR images, see Fig. 8. From Fig. 8, it can be observed that the algorithm can detect the dark spots well.

5. Conclusions

In this paper, a new algorithm for the detection of dark spots as the candidates of oil spills based on Poisson point process, Bayesian inference and Reversible Jump Markov Chain Monte Carlo algorithm have been presented. More precisely, in the proposed algorithm, the dark spots are modeled as marked point process which is created by a group of points uniformly drawing on the domain of a given image and attached a window with length, width and direction, and a gamma distribution with scale and shape parameters to each generating points.

Results from Radarsat-1 SAR intensity image show that the proposed algorithm can detect the dark spots very well. Instead of processing image pixel by pixel for the purpose of dark spot detection, the proposed algorithm processes the pixels in and out of windows simultaneously. Therefore, it is suitable for searching the oil spills on huge area. On the other hand, the proposed algorithm is a statistical region-based algorithm that can reduces the affect from speckle noise on the detection of dark spots.

In this paper we assume that the intensities of pixels on background (sea) follow identical independent gamma distributions with signal distribution parameters (α_0, β_0). Unfortunately, it is not always true due to the complicity of SAR imaging. The further work on improving the proposed algorithm will focuses on improving the proposed algorithm suitable for the scenes with non-uniform background.

Acknowledgments

The authors would like to thank Dr. Ziqiang Ou of Canadian Ice Service, Ottawa, for providing Radarsat-1 SAR data and the anonymous reviewers for their valuable comments.

References

Al-Awadhi, F., Jennison, C., & Hurn, M. (2004). Statistical image analysis for a confocal microscopy two-dimensional section of cartilage growth. *Applied Statistics, Journal of the Royal Statistical Society, Series C*, *53*(1), 31—49.

Benelli, G., & Garzelli, A. (1999). Oil spills detection in SAR images by fractal dimension estimation. *Proceeding of International Geoscience and Remote Sensing Symposium (IGARSS'99), Vol. 1* (pp. 218—220).

Besag, J. E., Green, P., Higdon, D., & Mengersen, K. (1995). Bayesian computation and stochastic systems (with discussion). *Statistical Science*, *10*, 3—66.

Brekke, C., & Solberg, A. H. S. (2005). Oil spill detection by satellite remote sensing. *Remote Sensing of Environment*, *95*(1), 1—13.

Chang, L. Y., Chen, K., Chen, C., & Chen, A. (1996). A multiplayer multiresolution approach to detection of oil slicks using ERS SAR image. *Proceeding of 17th Asian Conference of Remote Sensing (ACRS'96), Sri Lanka*.

Chen, C. F., Chen, K. S., Chang, L. Y., & Chen, A. J. (1997). The use of satellite imagery for monitoring coastal environment in Taiwan. *Proceeding of International Geoscience and Remote Sensing Symposium 1997 (IGARSS'97), Vol. 3* (pp. 1424—1426).

Derrode, S., & Mercier, G. (2007). Unsupervised multiscale oil slick segmentation from SAR images using a vector HMC model. *Pattern Recognition*, *40*(3), 1135—1147.

Descombes, X., & Zerubia, J. (2002). Marked point process in image analysis. *IEEE signal Processing Magazine*, *19*(5), 77—84.

Dryden, I., Scarr, M. R., & Taylor, C. C. (2003). Bayesian texture segmentation of weed and crop image using reversible jump Markov chain Monte Carlo methods. *Applied Statistics, Journal of the Royal Statistical Society, Series C*, *52*(1), 31—50.

Fingas, M. F., & Brown, C. E. (1997). Review of oil spill remote sensing. *Proceedings of the third International Airborne Remote Sensing Conference and Exhibition, 7–10 July 1997. Copenhagen, Denmark , Vol .I* (pp. 707—714).

Fiscella, B., Giancaspro, A., Nirchio, F., Pavese, P., & Trivero, P. (2000). Oil spill detection using marine SAR images. *International Journal of Remote Sensing*, *21*(18), 3561−3566.

Gilks, W. R., Richardson, S., & Spiegelhalter, D. J. (1996). Introducing Markov chain Monte Carlo. In W. R. Gilks, S. Richardson, & D. J. Spiegelhalter (Eds.), *Markov Chain Monte Carlo in Practice*. London: Chapman & Hall.

Green, J. (1995). Reversible jump Markov chain Monte Carlo computation and Bayesian model determination. *Biometrika*, *82*(4), 711−732.

Hartvig, N. V. (2002). A stochastic geometry model for functional magnetic resonance images. *Scandinavian Journal of Statistics*, *29*, 333−353.

Kanaa, T. F. N., Tonye, E., Mercier, G., Onana, V. P., Ngono, J. M., Frison, P. L., Rudant, J. P., & Garello, R. (2003). Detection of oil slick signature in SAR images by fusion of hysteresis thresholding responses. *Proceeding of International Geoscience and Remote Sensing Symposium 2003 (IGARSS'03), Vol. 4* (pp. 2750−2752).

Lee, J. S., Hoppel, K. W., Mango, S. A., & Miller, A. R. (1994). Intensity and phase statistics of multilook polarimetric and interferometric SAR imagery. *IEEE Transactions on Geoscience and Remote Sensing*, *32*, 1017−1028.

Lee, J. S., Jurkevich, I., Dewaele, P., Wambacq, P., & Oosterlinck, A. (1994). Speckle filtering of synthetic aperture radar images: a review. *Remote Sensing Review*, *8*, 313−340.

Liu, A. K., Peng, C. Y., & Chang, S. Y. (1997). Wavelet analysis of satellite images for costal watch. *IEEE Journal of Ocean Engineering*, *22*, 9−17.

Manore, M. J., Vachon, P. W., Bjerkelund, C., Edel, H. R., & Ramsay, B. (1998). Operational use of RADARSAT SAR in the coastal zone: the Canadian experience. *27th international Symposium on Remote Sensing of the Environment, Tromso, Norway, June 8–12*, 115−118.

Marghany, M., Hashim, M., & Cracknell, A. P. (2007). Fractal dimension algorithm for detecting oil spills using RADARSAT-1 SAR. In O. Gervasi & M. Gavrilova (Eds.), *Lecture Notes in Computer Science (LNCS) 4705* (pp. 1054−1062). Springer-Verlag: Berlin, Heidelberg.

Nirchio, F., Sorgente, M., Giancaspro, A., Biamino, W., Parisato, E., Ravera, R., & Trivero, P. (2005). Automatic detection of oil spills from SAR images. *International Journal of Remote Sensing*, *26*(6), 1157−1174.

Quartulli, M., & Datcu, M. (2004). Stochastic geometrical modeling for build-up area understanding from a single SAR intensity image with meter resolution. *IEEE Transactions on Geoscience and Remote Sensing*, *42*, 1996−2003.

Rue, H., & Hurn, M. A. (1999). Bayesian object identification. *Biometrika*, *83*(3), 649−660.

Schabenberger, O., & Gotway, C. A. (2005). *Statistical Methods for Spatial Data Analysis.* : Chapman & Hall/CRC Press.

Skϕelv, A., & Wahl, T. (1993). Oil spill detection using satellite based SAR. *Phase 1B Completion Report, Tech. rep., Norwegian Defence*.

Solberg, A. H. S., Dokken, S. T., & Solberg, R. (2003). Automatic detection of oil spills in Envisat, Radarsat and ERS SAR images. *Proceeding of International Geoscience and Remote Sensing Symposium 2003 (IGARSS'03), Vol. 4* (pp. 2747−2749).

Solberg, A. H. S., Storvik, G., Solberg, R., & Volden, E. (1999). Automatic detection of oil spill in ERS SAR images. *IEEE Transactions on Geoscience and Remote Sensing*, *37*, 1916−1924.

Stoyan, D., Kendall, W. S., & Mecke, J. (1995). *Stochastic geometry and its applications*, Second edition : John Wiley and Sons.

Topouzelis, K. (2008). Oil spill detection by SAR images: dark formation detection, feature extraction and classification algorithms. *Sensors*, *8*, 6624−6659.

Topouzelis, K., Karathanassi, V., Pavlakis, P., & Rokos, D. (2008). Dark formation detection using neural networks. *International Journal of Remote Sensing*, *29*, 4705−4720.

Vachon, P. W., Thomas, S. J., Cranton, J., Bjerkelund, C., Dobson, F. W., & Olsen, R. B. (1998). Monitoring the coastal zone with the RADARSAT satellite. *Ocenology International 98, UK, March, 10–13* 10 pp.

Wu, S. Y., & Liu, A. K. (2003). Towards an automated ocean feature detection, extraction and classification scheme for SAR imagery. *International Journal of Remote Sensing*, *24*, 935−951.